



## Article

# Design of a Compact, Planar, Wideband, Overlapped, Bow-Tie Antenna in a Single Layer with Stable Bi-Directional Radiation Patterns

Lauryn Smith <sup>1</sup>  and Sungkyun Lim <sup>2,\*</sup> 

<sup>1</sup> School of Electrical and Computer Engineering, Georgia Institute of Technology, Atlanta, GA 30332, USA; lsmith388@gatech.edu

<sup>2</sup> Department of Electrical and Computer Engineering, Georgia Southern University, Statesboro, GA 30460, USA

\* Correspondence: sklim@georgiasouthern.edu

**Abstract:** In this paper, a planar, bow-tie antenna with an enhanced bandwidth and a bi-directional radiation pattern is proposed. The concept of multi-resonance is applied by implementing the superposition of three different bow-tie components with various radii and flare angles in an overlapped fashion into a single element, resulting in a significant increase in bandwidth. The antenna has an electrical size,  $kr$ , of 1.10, calculated at the lowest frequency of operation. The proposed antenna is simulated, and a prototype is fabricated for verification by measurement. The result is a wide  $-10$  dB bandwidth of 80.3% (1.23–2.88 GHz) from the measurements. The antenna also maintains a bi-directional radiation pattern, with a negligible difference between the forward and backward realized gains, within the entire  $-10$  dB bandwidth. The measured realized gain values in the forward and backward directions are between 1.5 dBi and 3.7 dBi over the  $-10$  dB bandwidth. The comparison of the measurement and simulation results shows good agreement.

**Keywords:** bi-directional antennas; bow-tie antennas; electrically small antennas; planar antennas; printable antennas; wideband antennas



**Citation:** Smith, L.; Lim, S. Design of a Compact, Planar, Wideband, Overlapped, Bow-Tie Antenna in a Single Layer with Stable Bi-Directional Radiation Patterns. *Appl. Sci.* **2024**, *14*, 9555. <https://doi.org/10.3390/app14209555>

Academic Editors: Giovanni Maria Sardi and Walter Fuscaldo

Received: 14 September 2024

Revised: 14 October 2024

Accepted: 16 October 2024

Published: 19 October 2024



**Copyright:** © 2024 by the authors. Licensee MDPI, Basel, Switzerland. This article is an open access article distributed under the terms and conditions of the Creative Commons Attribution (CC BY) license (<https://creativecommons.org/licenses/by/4.0/>).

## 1. Introduction

As modern wireless devices perform a variety of functions simultaneously, they require multiple operating bands. There is a definite interest in the design of wideband antennas, since multiple narrowband antennas can be replaced with a single wideband antenna covering a range of frequencies while occupying a smaller volume. Although multiband antennas may be used to accommodate various frequency bands, wideband antennas are also desirable for their ability to transmit at high rates while having low input power requirements. However, conventional wideband antennas are typically large, since the bandwidth is increased when an antenna utilizes most of its encompassing sphere, which defines the electrical size,  $kr$ , of an antenna as the product of the wave number,  $k$  (evaluated at the lowest frequency in the bandwidth of the antenna), and the radius,  $r$ , of the encompassing sphere [1,2]. A variety of recently published wideband antennas require three-dimensional structures for enhanced bandwidth [3–6]. Planar or printable antenna designs, rather than three-dimensional geometries, are desirable in some applications due to the increasing compactness of wireless devices, their low cost, easy fabrication process, and the capability for mass production.

The bow-tie antenna, although it does not achieve as wide a bandwidth as a biconical antenna design due to its planarity, has become a cornerstone element for bandwidth enhancement in different kinds of antenna designs. The tapered design of the bow tie allows for impedance matching over a wide frequency range, resulting in a bandwidth that is tunable by adjusting the flare angle. Attempts have been made to reduce the size of

the bow-tie antenna while maintaining its wide bandwidth in [7–9]. In [7], a half bow-tie antenna was miniaturized—an integrated balun was applied on a truncated ground plane for improved bandwidth and gain. In [8], the size of the bow-tie antenna was reduced by 40% through the use of double-layering a folded bow tie and meander lines beneath the bow tie. In [9], the tips of the triangular bow-tie patch were removed for a more compact antenna structure. In [10], a wide bandwidth was demonstrated through implementing a rounded edge on a double-sided, bow-tie antenna. In [11–13], various alterations were made to the shape of the bow-tie slots, which required a large ground plane. These alterations were implemented to enhance the bandwidth of the antennas.

Previously, the multi-resonance principle has been used in a log-periodic dipole array (LPDA) antenna as a method for achieving a wide bandwidth. This method consists of scaled versions of the driver (fed) element combined into an array. Each individual element generates a resonance at a distinct frequency determined by its length. The summation of the resonances of each individual element results in a wide bandwidth. In [14–16], bow-tie antenna geometry was implemented for each element in the LPDA antenna to achieve an even wider bandwidth. However, the total sizes of these LPDA antennas were still large because the antennas required a large number of elements located next to each other with log-periodic distances in series. For example, in order to achieve more than 80% of  $-10$  dB bandwidth with LPDA antennas, at least six elements were required [17].

In this paper, an entirely planar (single layered), bandwidth-enhanced, single-element, bow-tie antenna is proposed. Contrary to previous designs using the multi-resonance principle, the antenna presented in this work is not an array. The single-element, shaped antenna design is realized through a combination of three different bow-tie components with various flare angles and radii, oriented to lay in the same plane, and centralized at the feed. Its enhanced bandwidth is achieved through the summation of the resonances of the individual components of the bow-tie elements. This configuration of overlapped bow ties occupies a much smaller area compared to the log-periodic array arrangement. The planarity and printability of the proposed antenna on  $50\ \mu\text{m}$  PET film allows for easy and cost-efficient fabrication—ideal for mass production. In addition, the electrical size (a  $kr$  of 1.10) of the proposed antenna is around 30% smaller than that of a full-sized,  $\lambda/2$  dipole. A genetic algorithm (GA) is used to optimize the dimensions of the antenna to increase its bandwidth. All the simulations are performed in CST Microwave Studio. Copper is chosen as the material for the simulation of the antenna. In Section 2, the detailed antenna design procedure is discussed. First, the effect of a varied flare angle and flare radius of the bow-tie antenna on its performance is studied. Next, the combination of the bow ties in an overlapped fashion is investigated, without and with a top-loading structure. In Section 3, the optimized design of the wideband, planar, bow-tie antenna composed of three bow-tie elements with different flare angles and flare radii is introduced, and the simulation results are provided. In Section 4, the measurement results are compared with the simulated ones for validation. The proposed antenna is also compared with other wideband, planar, bow-tie antennas from previous publications. The conclusions are stated in Section 5.

## 2. Antenna Design Procedure

The planar bow-tie antenna element is studied in terms of the flare angle through a simulation first. With a fixed flare radius,  $r$ , of 50 mm, various bow-tie antennas are designed with flare angles between  $40^\circ$  and  $160^\circ$ , in increments of  $40^\circ$ . The nomenclature for each antenna follows its flare angle—bow-tie-40 (Figure 1a), bow-tie-80 (Figure 1b), bow-tie-120 (Figure 1c), and bow-tie-160 (Figure 1d). As is evident, the vertical length of the bow tie decreases as the flare angle of the bow tie increases with the fixed radii. The simulated  $S_{11}$  (matched with a characteristic impedance of  $50\ \Omega$ ),  $R_{in}$ , and  $X_{in}$  for each of the aforementioned bow ties are shown in Figure 2a–c, respectively. The  $-10$  dB bandwidth, resonant frequency (defined as where  $X_{in}$  is  $0\ \Omega$  (Figure 2c)), and  $R_{in}$  (Figure 2b) at the resonant frequency, are examined for each bow tie. Bow-tie-40 and bow-tie-80 exhibit similar performances, with bandwidths of 20% and 22%, respectively. As the flare

angle is increased from  $40^\circ$  to  $80^\circ$ , there is a minor upward shift in the resonant frequency (1.16 GHz to 1.18 GHz) and a slight drop in  $R_{in}$  ( $56.7 \Omega$  to  $41.2 \Omega$ ). As the flare angle is further increased,  $R_{in}$  at the resonant frequency becomes smaller and smaller, resulting in an increase in the  $S_{11}$  values. For instance, bow-tie-120 has an  $R_{in}$  of  $18.4 \Omega$  at its resonant frequency of 1.36 GHz and, as a result, does not reach  $-10$  dB in  $S_{11}$ . Bow-tie-160 has a more significant reduction in  $R_{in}$ , with a value of  $4.1 \Omega$ , at its resonant frequency of 1.72 GHz, resulting in poor matching with the characteristic impedance of  $50 \Omega$ . The resonant frequency also shifts upward at a faster pace as the flare angle becomes larger and larger. This behavior is explained by a decreasing effective length, as the flare angle increases and the physical length of the antenna decreases. In Table 1, the aforementioned characteristics of each bow tie are summarized. A further investigation into the effect on the input impedance is provided here by observing the  $R_{in}$  and  $X_{in}$  of each bow tie in the angle study (Figure 1) at a single frequency, denoted by the vertical, black-dashed line in Figure 2b,c. The single frequency chosen for this study is 1.16 GHz—this is the resonant frequency of bow-tie-40, where  $X_{in}$  is equal to  $0 \Omega$ . As the flare angle increases at 1.16 GHz, both  $R_{in}$  and  $X_{in}$  decrease, and the bow-tie antenna becomes capacitive, similar to the behavior of a short dipole, due to the decrease in the vertical effective length of the antenna. The results for each flare angle studied are summarized in Table 2.

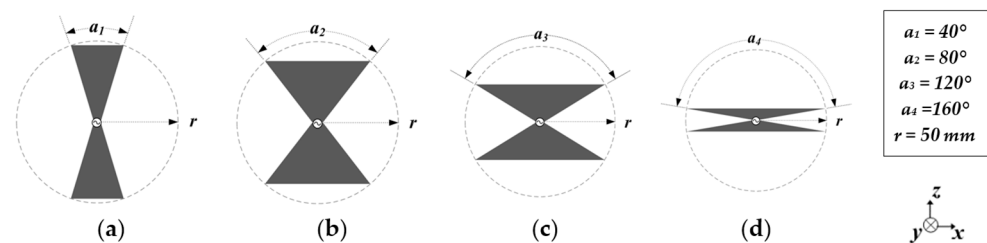


**Figure 1.** Dimensions and geometry of (a) bow-tie-40; (b) bow-tie-80; (c) bow-tie-120; and (d) bow-tie-160.

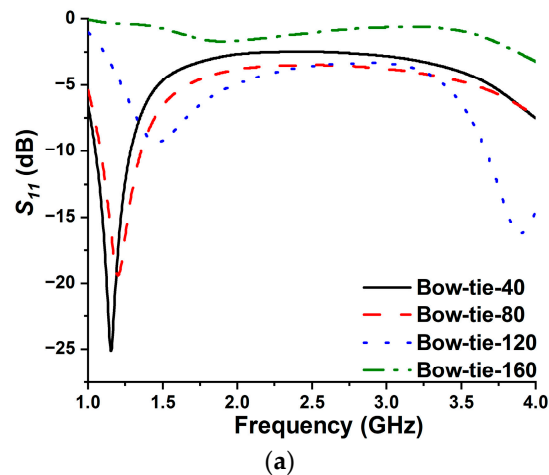


**Figure 2.** Cont.

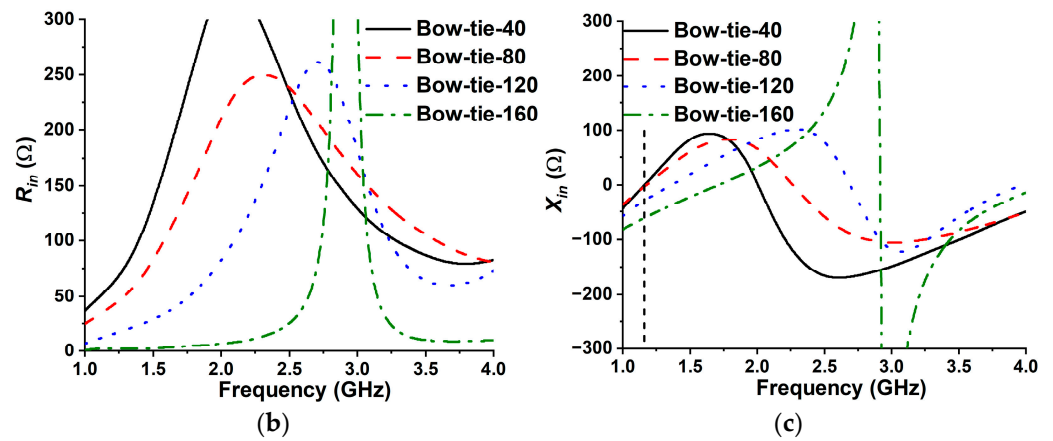


Figure 2. Simulated (a)  $S_{11}$ , (b)  $R_{in}$ , and (c)  $X_{in}$  for bow-tie-40, bow-tie-80, bow-tie-120, and bow-tie-160.

Table 1. Comparison of bow ties with different flare angles.

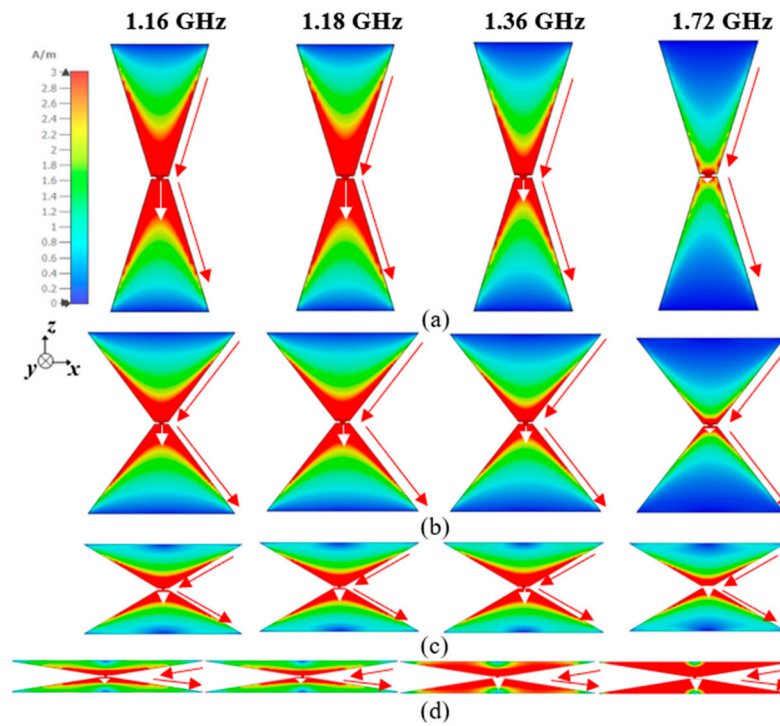
Antenna	$R_{in}$ ( $\Omega$ )	$X_{in}$ ( $\Omega$ )	Resonant Frequency (GHz)	−10 dB Bandwidth
Bow-tie-40	56.7	0	1.16	20.0%
Bow-tie-80	41.2	0	1.18	22.0%
Bow-tie-120	18.4	0	1.36	X
Bow-tie-160	4.1	0	1.72	X

Table 2. Comparison of input impedance of bow ties from angle study at 1.16 GHz.

Antenna	$R_{in}$ ( $\Omega$ )	$X_{in}$ ( $\Omega$ )
Bow-tie-40	56.7	0
Bow-tie-80	37.7	−3.7
Bow-tie-120	13.7	−29.6
Bow-tie-160	2.33	−61.5

Similar angle studies performed for other frequency ranges demonstrate that the same antenna characteristics apply regardless of the frequency range. Therefore, the antenna can be scaled up or down for operation in any frequency range.

To demonstrate the impact of the flare angle on the current distribution, Figure 3 shows the current distributions on each of the bow-tie antennas from the flare angle study (shown in Figure 1), at each of the resonances listed in Table 1 (1.16 GHz, 1.18 GHz, 1.36 GHz, and 1.72 GHz). The colored geometry depicts the current magnitude at each point along the bow-tie antenna, and the red arrows indicate the direction of the flow of the current, obtained from the simulation results. These arrows are only shown on the right side since the antenna design is symmetrical with respect to the z-axis. The white arrows are included to demonstrate how much of the center of the antenna’s geometry is covered by strong (red) currents with a value greater than 3 A/m. For a more exact investigation, the distance between the feed and the point where the current is 3 A/m (at the center of the geometry), is measured and summarized in Table 3. The dominant component at each frequency investigated is determined based on this distance.



**Figure 3.** Current distributions on (a) bow-tie-40, (b) bow-tie-80, (c) bow-tie-120, and (d) bow-tie-160 at 1.16 GHz, 1.18 GHz, 1.36GHz, and 1.72 GHz (left to right).

**Table 3.** Strong currents’ (3 A/m) distances from the feed.

Antenna	1.16 GHz	1.18 GHz	1.36 GHz	1.72 GHz
Bow-tie-40	<b>12.51 mm</b>	12.13 mm	6.37 mm	1.91 mm
Bow-tie-80	8.32 mm	<b>8.40 mm</b>	5.60 mm	2.57 mm
Bow-tie-120	6.06 mm	6.45 mm	<b>6.97 mm</b>	4.17 mm
Bow-tie-160	3.18 mm	3.27 mm	4.14 mm	<b>5.24 mm</b>

The bold is to highlight the importance of each bow-tie at each frequency.

Bow-tie-40 is shown in Figure 3a. As the frequency increases, the presence of the strong currents at the center of the antenna’s geometry decreases, demonstrating the resonance at 1.16 GHz, where the strong currents (greater than 3 A/m) extend a distance of 12.51 mm from the port. The current distributions for bow-tie-80 at each of the aforementioned frequencies are shown in Figure 3b—where a trend akin to the one in bow-tie-40 is shown. This further establishes the previous observation that the bow ties with two different flare angles (40° and 80°) are similar. The difference between the two is a slight shift in the resonant frequency, with strong currents predominant at 1.18 GHz for bow-tie-80. Bow-tie-120 is shown in Figure 3c, demonstrating resonance at 1.36 GHz, with the strong currents extending to a maximum distance of 6.97 mm. At all other frequencies, strong currents are less apparent. Lastly, the current distributions for bow-tie-160 are shown in Figure 3d. The presence of strong currents on bow-tie-160 increases as the frequency increases, and dominate at 1.72 GHz, with a maximum distance of 5.24 mm, demonstrating bow-tie-160’s resonance at this frequency. Thus, by increasing the flare angle, the frequency at which the largest area of the bow-tie geometry is covered in strong currents (coinciding with the resonant frequency) shifts to the right (increases).

Additionally, the effect of the flare radius on the resonant frequency is investigated through an observation of the simulated  $R_{in}$  and  $X_{in}$ , as shown in Figure 4a,b, respectively. In the flare radius study, a fixed flare angle of 160° is chosen based on the findings from the flare angle study—bow-tie-160 is important for extending the bandwidth in the upper end. Four different bow-tie antennas are investigated, having flare radii of 50 mm, 63 mm,

73 mm, and 83 mm. These radii values are chosen arbitrarily to establish a relationship between the flare radii and antenna performance. The nomenclature for the bow ties used in this study is followed by the respective flare radius in mm. For example, bow-tie-160-50 refers to the bow tie with a flare angle of  $160^\circ$  and a flare radius of 50 mm. As expected, while maintaining a constant flare angle of  $160^\circ$ , an increase in the flare radius reduces the resonant frequency, since the effective length of the antenna is increasing. With flare radii of 63 mm, 73 mm, and 83 mm, the resonance of the bow tie with a fixed flare angle shifts to 1.36 GHz, 1.18 GHz, and 1.04 GHz, respectively. In particular, it is noted that as the flare radius is increased, the slope of the  $R_{in}$  and  $X_{in}$  curves becomes steeper. For a wide bandwidth, a more gradual slope for the  $X_{in}$  curve is desired.

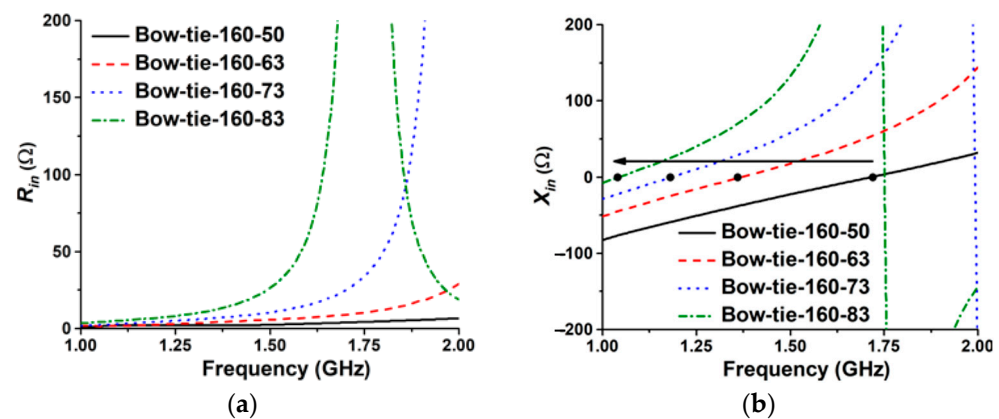


**Figure 4.** Simulated (a)  $R_{in}$  and (b)  $X_{in}$  for bow tie with flare angle of  $160^\circ$  and flare radius of 50 mm (bow-tie-160-50), 63 mm (bow-tie-160-63), 73 mm (bow-tie-160-73), and 83 mm (bow-tie-160-83).

Next, based on the multi-resonance principle, two variants of the triple bow-tie antenna, shown in Figure 5, are investigated. The triple bow tie in Figure 5a consists of three of the previously studied bow ties, bow-tie-80, bow-tie-120, and bow-tie-160, combined in an overlapped fashion and centralized at the feed. Ideally, the superposition of the  $S_{11}$  responses of each individual bow tie results in an enhanced  $-10$  dB bandwidth. Bow-tie-40 is not included in the overlapped bow tie, since the differences between bow-tie-40 and bow-tie-80 are negligible, in terms of  $R_{in}$ ,  $X_{in}$ , and the frequency shift. Bow-tie-80 is preferred since the  $-10$  dB bandwidth is slightly larger than that for bow-tie-40. Bow-tie-80, therefore, is included to supplement the lowest band, bow-tie-120 covers the middle band, and bow-tie-160 provides coverage in the highest band. Bow-tie-160 is especially important for bandwidth enhancement since, as determined by the flare angle study, as the flare angle increases the resonant frequency shifts to the right faster, facilitating a wider bandwidth.

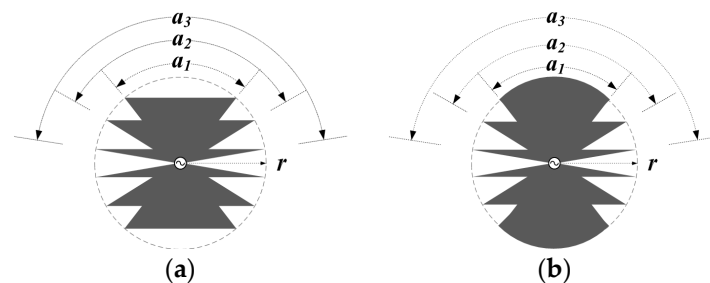


**Figure 5.** Dimensions and geometry of the triple bow ties of same radii and varying angles (a) without and (b) with a circular top.

The triple bow tie in Figure 5a fits within a sphere with a 50 mm radius and has an electrical size,  $kr$ , of 1.3. The simulated  $S_{11}$  is shown in Figure 6, and depicts a  $-10$  dB bandwidth enhancement with a value of 57.9% (1.24–2.25 GHz). Next, the triple bow tie



in Figure 5a is modified by the addition of a symmetrical circular top loading onto both ends of bow-tie-80, and is shown in Figure 5b. The effectiveness of circular top loadings on bow-tie antennas for bandwidth enhancement is demonstrated in [10]. The circular top loading provides an increased electrical length, allowing for the lowest frequency to be shifted even lower, generating a broader bandwidth as shown in Figure 6. The antenna now has a  $-10$  dB bandwidth of 65.4% (1.08–2.13 GHz) and a smaller electrical size (1.13), since it is calculated at the lowest frequency in the bandwidth of the antenna.

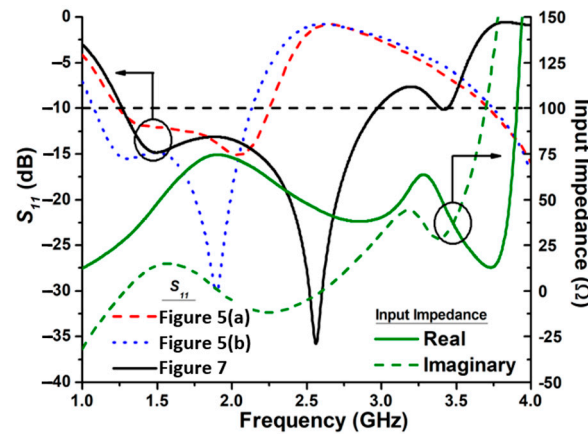


**Figure 6.** Simulated  $S_{11}$  for the triple bow ties with the same radius, without (Figure 5a) and with circular top loading (Figure 5b), and for the proposed wideband, planar, bow-tie antenna (Figure 7), and the simulated input impedance of the proposed wideband, planar, bow-tie antenna.

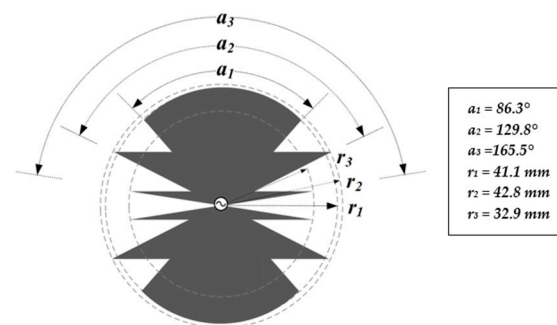


**Figure 7.** Dimensions and geometry of the proposed wideband, planar, bow-tie antenna.

### 3. Proposed Wideband, Planar, Bow-Tie Antenna

The final antenna design and its dimensions are shown in Figure 7. The proposed bow-tie antenna is entirely planar—there are no multilayered components, and the antenna lays in one plane (the XZ plane). The dimensions are optimized using a genetic algorithm (GA) optimization. Since the radiation pattern of the antenna is bi-directional, meaning that there is a negligible difference between the frontwards and backwards realized gains, the cost function is simplified to include  $S_{11}$  only to maximize the  $-10$  dB bandwidth as follows:

$$\text{Cost Function} = \sum_{f_l=1.0}^{f_h=3.0} (S_i - (-15)) \text{ (dB)}, \quad (1)$$

where  $S_i$  is the  $S_{11}$  (dB) value at various frequencies between  $f_l$  (1.0 GHz) and  $f_h$  (3.0 GHz) [18]. The GA uses the flare angle and radii of each constituent bow tie as the variables, contrary to the designs in Figure 5, where the radius of each bow tie is the same. These variables are constrained to ensure that the geometry always comprises three distinct bow ties. The nomenclature of the three different bow ties follows the pattern established in Section 2, where each name corresponds to the flare angle of the constituent bow tie (rounded to the nearest whole number). The longest bow tie (bow-tie-86) has a radius of 41.1 mm and

an angle of  $86.3^\circ$  and the circular top loading has the same radius. The middle bow tie (bow-tie-130) has the largest radius, 42.8 mm, and an angle of  $129.8^\circ$ . Finally, the shortest bow tie (bow-tie-166) has a radius of 32.9 mm and the largest angle,  $165.5^\circ$ .

Since the radius of bow-tie-86 is slightly decreased to 41.1 mm, compared to that of bow-tie-80 in Section 2, the lowest frequency in the  $-10$  dB bandwidth is slightly shifted to the right, as shown in Figure 6. However, a bandwidth increase of 14.8% on the upper end, compared to that for the design in Figure 5b, is shown. This is because of the increased angle ( $166^\circ$ ) paired with the decreased radius (32.9 mm) of bow-tie-166, compared to bow-tie-160 in Section 2.

Consequently, the superposition of these bow ties with varying flare angles and radii paired with circular top loading generates the oscillation of  $R_{in}$  at around  $50 \Omega$ , and  $X_{in}$  at around  $0 \Omega$ , as depicted in Figure 6. This leads to a wider impedance bandwidth of 80.2% (1.26–2.97 GHz), compared to that of the initial design shown in Figure 5a, valued at 57.9% (1.24–2.25 GHz).

The proposed antenna is studied at four evenly spaced frequencies within the  $-10$  dB bandwidth of the presented antenna—1.26 GHz (the lowest frequency), 1.84 GHz (one-third of the  $-10$  dB bandwidth), 2.41 GHz (two-thirds of the  $-10$  dB bandwidth), and 2.97 GHz (the highest frequency)—to investigate the contribution of each bow tie to the wider bandwidth, shown in Figure 8a–d, respectively. Some important featured areas of the strong currents are indicated by the black circles and the black arrows next to them, to show the direction of the strong currents. These indicators are only shown on the right side of each antenna since the antenna is symmetrical across the z-axis. The blue and red circles represent the first and second nulls, respectively, where the currents traveling in different directions cancel each other out. The double-sided, blue arrows between the first null and the feed indicate the distance between them.

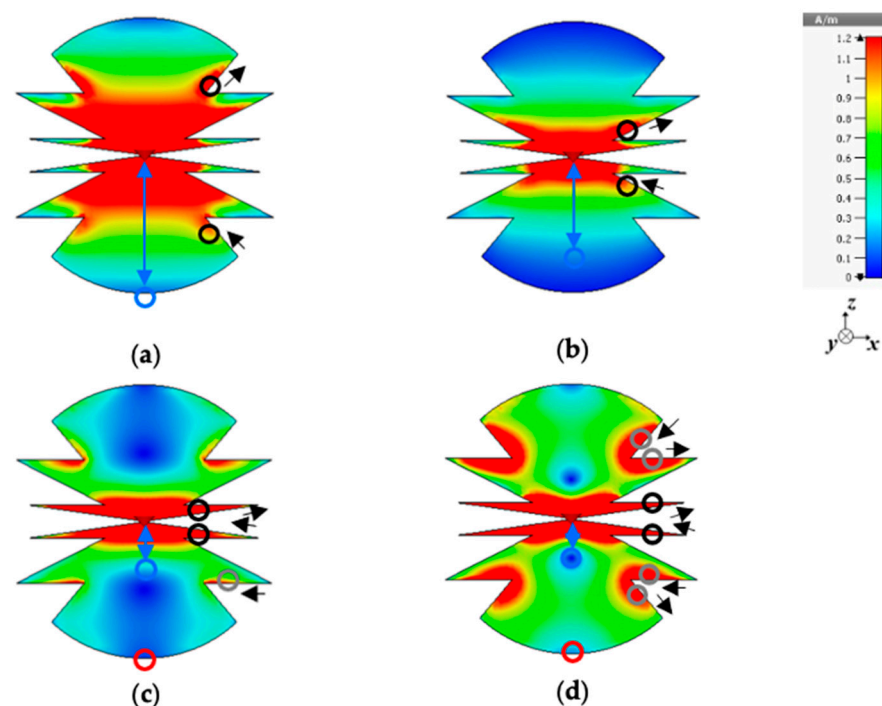


**Figure 8.** Current distributions at (a) 1.26 GHz, (b) 1.84 GHz, (c) 2.41 GHz, and (d) 2.97 GHz (left to right).

The main operating component of the proposed bow-tie antenna at each of the previously mentioned frequencies is determined based on the featured strong currents shown in black circles in Figure 8. At 1.26 GHz, the strongest currents are highlighted on bow-tie-86 in Figure 8a. Bow-tie-130 has strong currents on the majority of its area at 1.84 GHz, shown in Figure 8b. Finally, the entire surface area of the single bow-tie-166 is covered in



strong currents at 2.41 GHz and 2.97 GHz, shown in Figure 8c,d, respectively. This demonstrates that bow-tie-86 is the main operating component at 1.26 GHz (lower frequency range), bow-tie-130 at 1.84 GHz (the middle frequency range), and bow-tie-166 at 2.41 GHz and 2.97 GHz (the higher frequency range), confirming the operating principle that each bow tie contributes to the wide bandwidth, through the superposition of their individual impedance bandwidths.

It is also observed that the first null (indicated by the blue circle) on bow-tie-86 (Figure 8a,b) moves towards the feed gradually as the frequency increases, and that the second null (indicated by the red circle) appears from 2.41 GHz, demonstrating the harmonics of bow-tie-86. At 2.41 GHz and 2.97 GHz, the grey circles in Figure 8c,d highlight the emergence of strong currents traveling in the opposite direction on the top and bottom edges of bow-tie-130, due to the harmonics of bow-tie-86 and bow-tie-130 at this frequency. This results in a minor alteration in the radiation pattern at 2.41 GHz and 2.97 GHz, which is shown in Section 4.

#### 4. Comparison between Simulation and Measurement

Further investigation into the simulated characteristics of the proposed antenna design is provided and verified through measurement. The proposed planar, wideband, bow-tie antenna is fabricated by etching copper onto a flexible 50  $\mu\text{m}$  thick PET film, which has a permittivity of 3.3 and a loss tangent of 0.005. The prototype, shown in Figure 9, is then measured in an anechoic chamber using a 180°, -3 dB hybrid coupler (Krytar 4005070) operating from 0.5 to 7 GHz as a balun [19]. Two input ports of the hybrid coupler are 180° out of phase with each other. These ports are connected to SMA cables, which are soldered together on the sides. The open end of each cable is soldered to each arm of the prototype, as shown by the silver dots of the soldering material on the center of the fabricated antenna in Figure 9. The hybrid coupler also has two output ports—the summing port and the differential port. The summing port is terminated by a 50  $\Omega$  load and the differential port is connected to an Agilent E5071C network analyzer to record the measurement data. The measurement of the wideband, planar, bow-tie antenna in an anechoic chamber is shown in Figure 10.

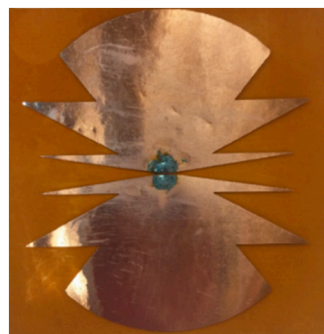


Figure 9. The prototype of the proposed wideband, planar, bow-tie antenna.

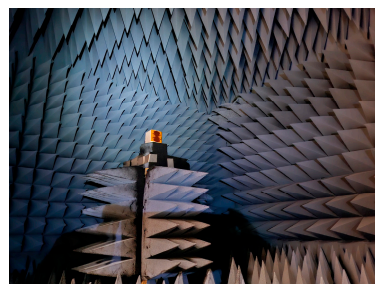
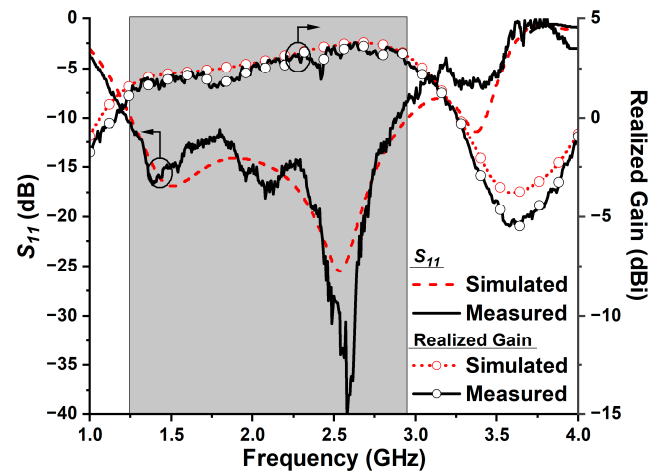


Figure 10. The measurement of the proposed wideband, planar, bow-tie antenna in an anechoic chamber.

The measured  $S_{11}$  is shown in Figure 11, overlapped with the simulated one. From the measurement, the  $-10$  dB bandwidth is 80.3% (1.23–2.88 GHz), and matches well with the simulation results (highlighted by the grey area) of 80.2% (1.26–2.97 GHz). Since the PET supporting structure is extremely thin, it has a negligible effect on the antenna performance, as demonstrated by the similarity between the simulation (where the PET film is not included) and the measurement (where the PET film is used to support the antenna) results. The simulated and measured forward realized gains are also shown in Figure 11. The simulation results confirm that the backward realized gain is identical to the forward realized gain, and, therefore, the backward realized gain is omitted in Figure 11. Both the simulation and measurement results show that a steady realized gain is maintained throughout the  $-10$  dB bandwidth, with simulated values of 1.6–3.8 dBi and measured values of 1.5–3.8 dBi. The measurement results agree well with those of the simulation.



**Figure 11.** Simulated and measured  $S_{11}$  and forward realized gain of the proposed wideband, planar, bow-tie antenna.

The measured radiation patterns at the lowest frequency (1.26 GHz), at one-third of the  $-10$  dB bandwidth (1.84 GHz), at two-thirds of the  $-10$  dB bandwidth (2.41 GHz), and at the highest frequency (2.97 GHz) are compared with the simulated ones in Figure 12. The simulated XY-plane radiation patterns are also shown in Figure 12 for a comprehensive view. The proposed antenna design is linearly polarized. For each frequency, the radiation patterns in both the XZ plane (parallel to the plane the antenna lies in) and YZ plane (perpendicular to the plane of the antenna) are shown.

Overall, the simulation and measurement results match fairly well. Bi-directionality is demonstrated at each of the frequencies investigated. As previously mentioned, the opposing currents on bow-tie-86 and bow-tie-130 shown in Figure 8d result in a minor distortion of the radiation pattern at the highest frequency (2.97 GHz) of the  $-10$  dB bandwidth in the XZ plane (Figure 12d), and a gradual loss of omnidirectionality in the XY plane as the frequency increases.

Finally, previously published works on wideband, bow-tie antennas, with the criteria limited to planar, bow-tie antennas, including both single and multilayered ones, are compared with the proposed antenna in Table 4. The criteria for the references included in this comparison table does not limit the directionality (both bi-directional and uni-directional designs are included), since the main goal of the proposed antenna is improving the bandwidth of the bow-tie antenna while maintaining a planar, relatively small size—rather than the directionality of the antenna. The overall size, in terms of  $\lambda$ , and the electrical size ( $kr$ ) for each antenna are calculated at the lowest frequency in the  $-10$  dB bandwidth. The proposed wideband, planar, bow-tie antenna has the smallest electrical size, aside from the half bow-tie antenna design in [7], which has a narrower bandwidth and lower gain.

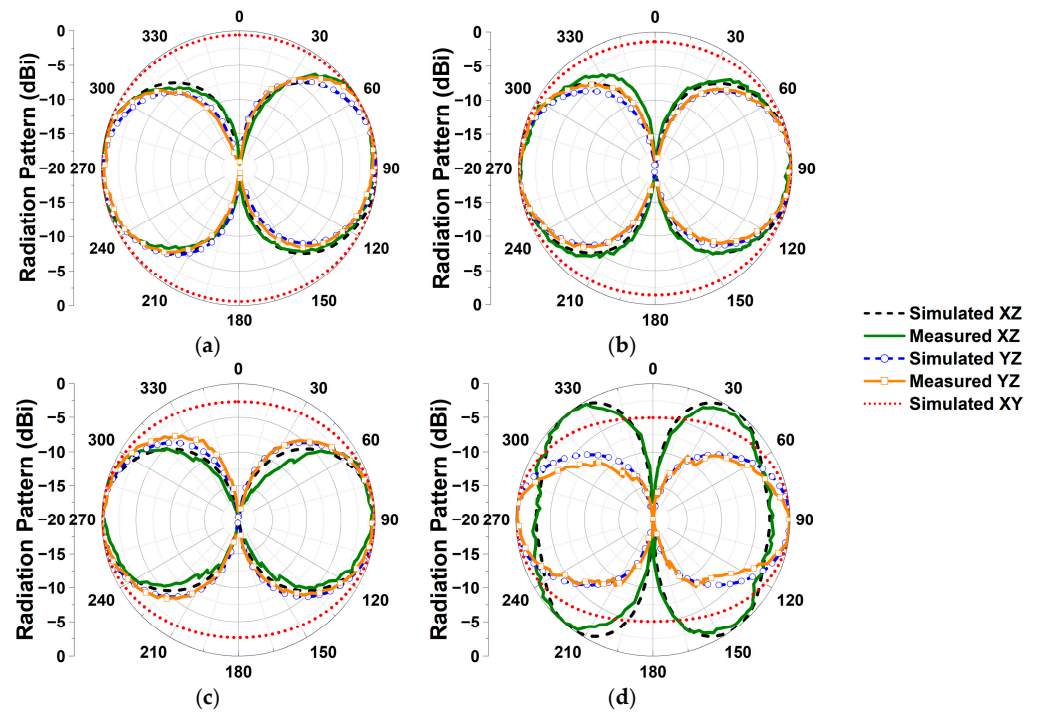


**Figure 12.** Simulated and measured radiation patterns of the proposed wideband, planar, bow-tie antenna in the XZ, YZ, and XY planes at (a) 1.26 GHz, (b) 1.84 GHz, (c) 2.41 GHz, and (d) 2.97 GHz.

**Table 4.** Comparison of wideband, planar, bow-tie antennas.

Ref.	Multi-Layered?	Directionality	−10 dB Bandwidth	Overall Size (m)	Electrical Size (kr)	Peak Gain (dBi)	Peak Realized Gain (dBi)
[7]	No	Bi-directional	47.0% (2.30–3.70 GHz)	$0.280\lambda \times 0.146\lambda \times 0.006\lambda$	0.99	2.6	-
[9]	Yes	Bi-directional	117.6% (2.75–10.60 GHz)	$0.330\lambda \times 0.330\lambda \times 0.012\lambda$	1.47	3.4	-
[10]	Yes	Bi-directional	114.3% (3.00–11.00 GHz)	$0.360\lambda \times 0.360\lambda \times 0.013\lambda$	1.60	5.2	-
[11] <sup>a</sup>	No	Bi-directional	71.4% (2.70–5.70 GHz)	$0.656\lambda \times 0.380\lambda \times 0.014\lambda$	2.38	-	7.0
[11] <sup>b</sup>	No	Bi-directional	90.3% (1.70–4.50 GHz)	$0.516\lambda \times 0.301\lambda \times 0.009\lambda$	1.88	-	6.0
[12]	No	Bi-directional	54.0% (4.67–8.13 GHz)	$1.203\lambda \times 0.697\lambda \times 0.001\lambda$	4.37	7.7	-
[13]	No	Bi-directional	98.3% (2.76–51.40 GHz)	$0.488\lambda \times 0.232\lambda \times 0.015\lambda$	1.69	5.5	-
[14]	Yes	Uni-directional	51.4% (5.98–10.12 GHz)	$0.558\lambda \times 0.897\lambda \times 0.016\lambda$	3.32	5.3	-
[15]	Yes	Uni-directional	33.7% (36.60–51.54 GHz)	$1.233\lambda \times 2.183\lambda \times 0.063\lambda$	7.88	12.5	-
[20]	No	Bi-directional	57.7% (2.20–3.99 GHz)	$0.587\lambda \times 0.440\lambda \times 0.002\lambda$	2.30	6.9	-
[21]	Yes	Uni-directional	171.2% (3.10–40.00 GHz)	$0.620\lambda \times 0.444\lambda \times 0.016\lambda$	2.40	7.1 <sup>c</sup>	-
[22]	Yes	Uni-directional	40.0% (3.80–5.70 GHz)	$0.926\lambda \times 1.089\lambda \times 0.020\lambda$	4.49	5.0	-
[23]	Yes	Uni-directional	35.0% (7.26–10.34 GHz)	$1.095\lambda \times 0.973\lambda \times 0.012\lambda$	4.60	6.1	-
Proposed Antenna	No	Bi-directional	80.3% (1.26–2.97 GHz)	$0.350\lambda \times 0.330\lambda \times 0.001\lambda$	1.10	3.8	3.7

Note: All the values are from the simulations since some references do not include measurement results. The overall size and electrical size are calculated using the lowest frequency in the −10 dB bandwidth. <sup>a</sup> Smaller physical size version. However, since it has a higher frequency than the wider bandwidth version, the electrical size is larger. <sup>b</sup> Wider bandwidth version. <sup>c</sup> The value is from a measurement since the value from a simulation is not provided.

Undeterred by its relatively small size, compared to the antennas from the references included in the table, the proposed antenna still exhibits a competitive  $-10$  dB bandwidth (four times the bandwidth of the conventional bow-tie antenna with a similar electrical size,  $kr$ , of 1.12, investigated in Section 2) with a stable realized gain throughout the bandwidth. The antenna does not require any ground plane. Since the proposed antenna is single layered (purely two dimensional) and can be printed on a flexible film, it may potentially provide bending insensitivity, similar to the antenna design in [20].

## 5. Conclusions

In this article, a planar, bow-tie antenna comprising three distinct bow-tie geometries superposed in an overlapped fashion is presented for wideband applications. The antenna has an area of  $85.6 \text{ mm} \times 82.2 \text{ mm}$  ( $0.35\lambda \times 0.33\lambda$ ) and a  $kr$  of 1.10, calculated at the lowest frequency in the  $-10$  dB bandwidth. Based on the concept of the multi-resonances principle, the superposition of three different bow ties paired with circular top loading results in an enhanced  $-10$  dB bandwidth of 80.3% (1.23–2.88 GHz) from the measurement. The antenna maintains a steady bi-directional radiation pattern and a realized gain of 1.5–3.8 dBi over its entire bandwidth. The antenna is fabricated and measured for verification. The proposed antenna design does not require any ground plane and since its design is two dimensional, it can be printed on a thin film for potential use as a flexible antenna for conformal applications, wearable antennas and smart textiles, drones, and energy harvesting. Its wide bandwidth capabilities allow for high data transmission rates, and the simultaneous transmission of multiple signals at different frequencies with no interference, supporting multiple functions (for example, localization, communication, etc.) with a single antenna.

**Author Contributions:** Data curation, L.S.; writing—original draft preparation, L.S.; writing—review and editing, S.L.; supervision, S.L. All authors have read and agreed to the published version of the manuscript.

**Funding:** This research received no external funding.

**Institutional Review Board Statement:** Not applicable.

**Informed Consent Statement:** Not applicable.

**Data Availability Statement:** The data presented in this study are available on request from the corresponding author.

**Conflicts of Interest:** The authors declare no conflict of interest.

## References

1. Harrington, R.F. Effect of antenna size on gain, bandwidth and efficiency. *J. Res. Natl. Inst. Stand. Technol.* **1960**, *64D*, 1–12.
2. Chu, L.J. Physical limitations of omni-directional antennas. *J. Appl. Phys.* **1948**, *19*, 1163–1175. [[CrossRef](#)]
3. Yeoh, W.S.; Rowe, W.S.T. An UWB conical monopole antenna for multiservice wireless applications. *IEEE Antennas Wirel. Propag. Lett.* **2015**, *14*, 1085–1088. [[CrossRef](#)]
4. Zhekov, S.S.; Tatomirescu, A.; Pederson, G.F. Antenna for ultrawideband channel sounding. *IEEE Antennas Wirel. Propag. Lett.* **2016**, *16*, 692–695. [[CrossRef](#)]
5. Aten, D.W.; Haupt, R.L. A wideband, low profile, shorted top hat monocone antenna. *IEEE Trans. Antennas Propag.* **2012**, *60*, 4485–4491. [[CrossRef](#)]
6. Liu, A.; Lu, Y. A superwide bandwidth low-profile monocone antenna with dielectric loading. *IEEE Trans. Antennas Propag.* **2019**, *67*, 4173–4177. [[CrossRef](#)]
7. Yeoh, W.S.; Wong, K.L.; Rowe, W.S.T. Wideband miniaturized half bowtie printed dipole antenna with integrated balun for wireless applications. *IEEE Trans. Antennas Propag.* **2011**, *59*, 339–342. [[CrossRef](#)]
8. Li, X.; Jalilvand, M.; Sit, Y.L.; Zwick, T. A compact double-layer on-body matched bowtie antenna for medical diagnosis. *IEEE Trans. Antennas Propag.* **2014**, *62*, 1808–1816. [[CrossRef](#)]
9. Kiminami, K.; Hirata, A.; Shiozawa, T. Double-sided printed bow-tie antenna for UWB communications. *IEEE Antennas Wirel. Propag. Lett.* **2004**, *3*, 152–153. [[CrossRef](#)]
10. Karacolak, T.; Topsakal, E. A double-sided rounded bow-tie antenna (DSRBA) for UWB communication. *IEEE Antennas Wirel. Propag. Lett.* **2006**, *5*, 446–449. [[CrossRef](#)]

11. Bhaskar, V.S.; Tan, E.L.; Holden, L.K.H. Design of wideband bowtie slot antenna using sectorially modified gielis curves. *IEEE Antennas Wirel. Propag. Lett.* **2018**, *17*, 2237–2240. [[CrossRef](#)]
12. Pierce, R.G.; Blanchard, A.J.; Henderson, R.M. Broadband planar modified aperture bowtie antenna. *IEEE Antennas Wirel. Propag. Lett.* **2013**, *12*, 1432–1435. [[CrossRef](#)]
13. Xu, L.; Li, L.; Zhang, W. Study and design of broadband bow-tie slot antenna fed with asymmetric CPW. *IEEE Trans. Antennas Propag.* **2015**, *63*, 760–765. [[CrossRef](#)]
14. Qu, S.; Li, J.; Xue, Q.; Chan, C. Wideband periodic endfire antenna with bow-tie dipoles. *IEEE Antennas Wirel. Propag. Lett.* **2008**, *7*, 314–317.
15. Chu, Q.; Li, X.; Ye, M. High-gain printed log-periodic dipole array antenna with parasitic cell for 5G communication. *IEEE Trans. Antennas Propag.* **2017**, *65*, 6338–6344. [[CrossRef](#)]
16. Gao, X.; Shen, Z.; Hua, C. Conformal VHF log-periodic balloon antenna. *IEEE Trans. Antennas Propag.* **2015**, *63*, 2756–2761. [[CrossRef](#)]
17. Smith, L.P.; Howell, J.C.; Lim, S. A size-reduced, 15-element, planar Yagi antenna. *IEEE Trans. Antennas Propag.* **2021**, *69*, 2410–2415. [[CrossRef](#)]
18. Chen, J.; Ludwig, J.; Lim, S. Design of a Compact Log-Periodic Dipole Array Using T-Shaped Top Loadings. *IEEE Antennas Wireless Propag. Lett.* **2017**, *16*, 1585–1588. [[CrossRef](#)]
19. Krytar, Model 4005070, Frequency Band: 0.5 GHz~7 GHz 180° Hybrid Coupler. Available online: <https://krytar.com/wp-content/uploads/2022/05/4005070.pdf> (accessed on 14 September 2024).
20. Sallam, M.O.; Kandil, S.M.; Volski, V.; Vandenbosch, G.A.; Soliman, E.A. Wideband CPW-fed flexible bow-tie slot antenna for WLAN/WiMax systems. *IEEE Trans. Antennas Propag.* **2017**, *65*, 4274–4277. [[CrossRef](#)]
21. Yurduseven, O.; Smith, D.; Elsdon, M. Printed slot loaded bow-tie Antenna with Super Wideband Radiation Characteristics for Imaging applications. *IEEE Trans. Antennas Propag.* **2013**, *61*, 6206–6210. [[CrossRef](#)]
22. Ake, W.D.; Pour, M.; Mehrabani, A. Asymmetric half-bowtie antennas with tilted beam patterns. *IEEE Trans. Antennas Propag.* **2019**, *67*, 738–744.
23. Feng, C.; Shi, T.; Wang, L. Novel broadband bow-tie antenna based on complementary split-ring resonators enhanced substrate-integrated waveguide. *IEEE Access* **2009**, *7*, 12397–12404. [[CrossRef](#)]

**Disclaimer/Publisher’s Note:** The statements, opinions and data contained in all publications are solely those of the individual author(s) and contributor(s) and not of MDPI and/or the editor(s). MDPI and/or the editor(s) disclaim responsibility for any injury to people or property resulting from any ideas, methods, instructions or products referred to in the content.